Journal of Himalayan Earth Sciences Volume 59, No. 1, 2026 pp. 1-21

Mineralogical and Geochemical Investigation of Sulfide Mineralization in Ushiri Valley, Western Kohistan Island Arc, Pakistan: Implications for Genesis

Israr Ud Din[1*], Asghar Ali[2], Mohammad Tahir Shah[1], and Muhammad Farhan[3]

[1] *National Centre of Excellence in Geology, University of Peshawar 25130, Pakistan*

[2] *Department of Geology, University of Peshawar, Pakistan*

[3] *Department of Marine Sciences, Zhejiang University, Zhoushan, 316021, PR China*

**Corresponding author: isrargeo01@gmail.com*

Submitted date: 06/09/2024 Accepted date: 06/02/2025 Published online: 31/03/2026

Abstract

The Ushiri Valley sulfide mineralization, a newly identified deposit in the Upper Dir region, is located in the western part of the Kohistan Island Arc, northern Pakistan. The mineralization occurs within massive amphibolites of the Kamila Amphibolites and the granodiorite and granite of the Kohistan Batholith. Three types of mineralization have been identified: 1) sulfide mineralization along quartz veins, 2) disseminated sulfide mineralization in the host rocks, and 3) supergene enrichment along localized shear zones. The amphibolites, granodiorite, and granite of the study area are extensively intruded by quartz veins, which generally host sulfide mineralization mainly in the form of chalcopyrite and pyrite, with a lesser amounts of bornite, galena, and sphalerite. Secondary minerals such as malachite, azurite, and limonite/hematite occur as products of supergene enrichment. The host rocks adjacent to the mineralized quartz veins contain the same sulfide mineral assemblage in disseminated form. Hydrothermal alteration, including saussuritization, sericitization, kaolinization, propylitization, and silicification is commonly observed in the mineralized host rocks within shear zones and at the contact between mineralized quartz veins and the host rocks. Geochemical data from hydrothermally altered host rocks indicate that the mineralizing hydrothermal fluids were significantly enriched in FeO, K_2O, and Cu, while the Pb, Zn, W, Cr, Ni, and Co show slight enrichment. Sulfur ($\delta^{34}S$) and oxygen ($\delta^{18}O$) isotopic data suggest the involvement of heavy magmatic fluids related to deep-seated intrusions. These fluids likey formed metal complexes and acted as high-temperature metalliferous fluids responsible for the precipitation of base metals sulfides within quartz veins and the associated host rocks, which can be correlated with a porphyry-type mineralizaton system.

Keywords: Sulfide mineralization; hydrothermal alteration; S-O isotopes; magmatic-hydrothermal fluids.

1. Introduction

Island arcs are considered favorable sites for the formation of magmatic-hydrothermal deposits such as volcanic massive sulfide deposits, epithermal Au–Ag deposits, and porphyry Cu–Mo–Au deposits (Mitchell and Bell, 1973; Brown et al., 2011; Farhan et al., 2023). The Kohistan Island Arc (KIA) in northern Pakistan formed due to the intra-oceanic subduction of the Neo-Tethys Ocean and represents a complex geological history of crustal evolution (Bignold & Treloar, 2003; Bignold et al., 2006).

These geological processes created favorable conditions for the formation of various mineral deposits, including precious- and base-metal placer deposits along the Indus River, hydrothermal copper mineralization, epithermal Au–Ag deposits, and porphyry Cu–Mo–Au deposits (Kausar, 1991; Shah, 1994, 1997; Shah et al., 1994;

Ali, 2011; Tahirkheli et al., 2012; Alam et al., 2019; Hussain et al., 2020; Farhan et al., 2021).

The study area forms part of Ushiri Valley, located in the western part of the Kohistan Island Arc in northern Pakistan. Metallic mineralization in the area occurs mainly within quartz veins and adjacent host rocks such as amphibolites, granodiorites, and granites. Although the geology and geochemistry of these rocks have previously been investigated (Shah et al., 2000), detailed mineralogical, geochemical, and genetic studies of the associated sulfide mineralization are lacking.

Therefore, the present study aims to investigate the genesis of sulfide mineralization in the study area based on detailed field observations, petrographic analysis, mineralogical characterization, and geochemical investigations, including oxygen and sulfur isotopic analyses.

2. Regional and local geological settings

Northern Pakistan contains a record of continental collisions and a complex geological history. Geotectonically, north Pakistan is divided into three domains: from south to north the Indo-Pakistan plate, the KIA, and the Karakoram block (Ullah et al., 2023; Zafar et al., 2023) (Fig. 1). The KIA is bounded by two suture zones, in the north by Shyok Suture Zone /Main Karakoram Thrust and in the south by Indus Suture Zone/Main Mantle Thrust (Coward et al., 1987; Petterson, 2010; Zafar et al., 2023). The KIA is one of the unique examples of an intra-oceanic island arc, showing a complete section ranging from the upper mantle to the uppermost sedimentary layer (Petterson, 2010). From south to north, it comprises the ultramafic–mafic Jijal-Sapat Complex, Kamila Amphibolites, Chilas Complex, Kohistan Batholith, Chalt volcanic, and Gilgit Metasedimentary rocks (Khan et al., 1993).

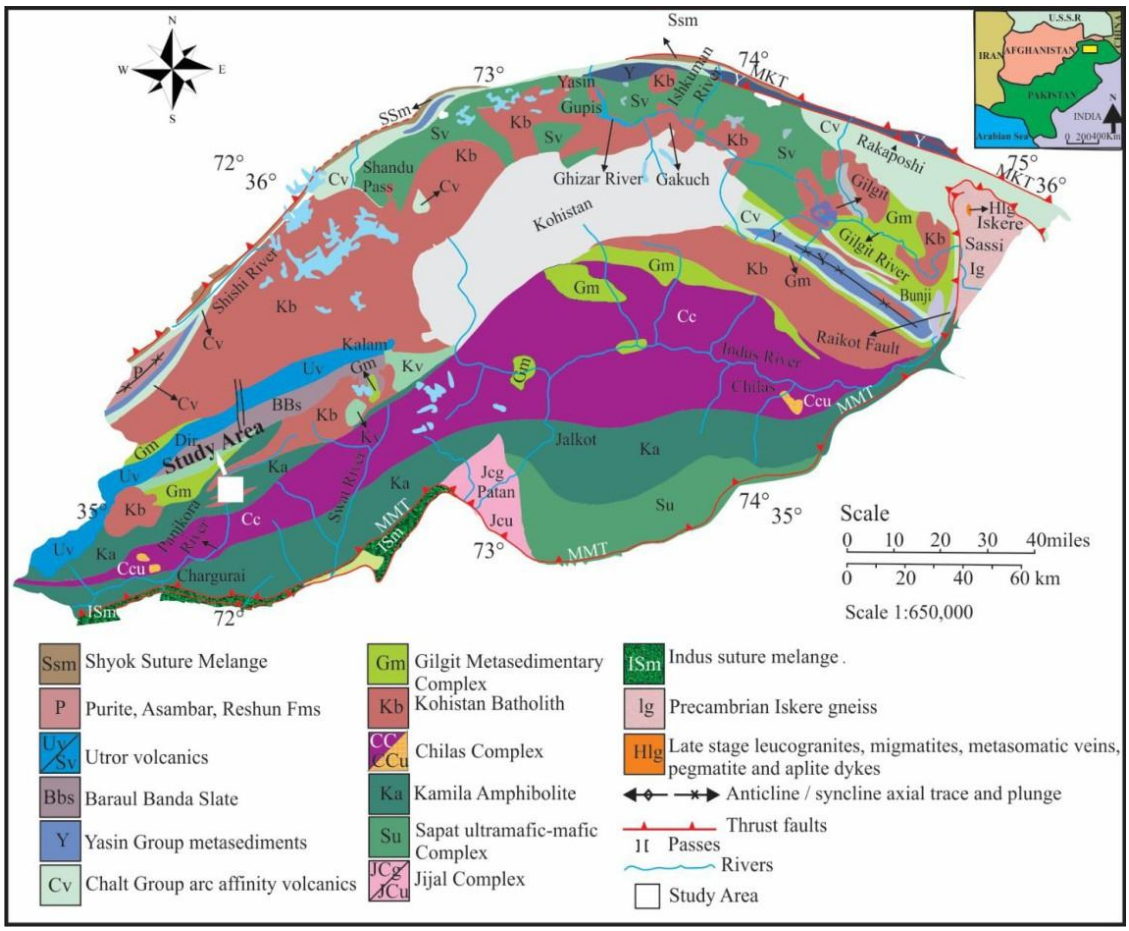

Fig. 1. Geological map of Kohistan island arc adopted from Zanchi and Gaetani (2011). The study area is located in the western part of the Kohistan island arc as shown on the map.

The study area consists of Kamila amphibolite in the south and the granites and granodiorites of Kohistan batholith in the north (Fig. 2). Amphibolites are medium to coarse-grained rocks with massive, banded and foliated textures. Hornblende and plagioclase are the dominant, quartz is the minor constituents while biotite, muscovite, chlorite, epidote, apatite, sphene, rutile and opaque minerals occur as accessories in these rocks. The medium to coarse-grained granodiorites and granites, having a sharp intrusive contact with amphibolites, are dominated by weak foliation, angular joints, local faulting, and fractures. Granodiorites are dominantly composed of alkali feldspar, plagioclase and quartz with a minor amount of biotite, muscovite, zircon and opaque occur as accessories. Granites are mainly composed of quartz, Alkali feldspar and plagioclase while muscovite, chlorite, hornblende, augite and opaque occur as accessories. These rocks are sheared at places and attained schistosity along the shear zone where the epidotization is prominent.

All these rocks (i.e., amphibolites, granites and granodiorites) are sheared at places and are intruded by the quartz and quartzo-feldspathic veins. The quartz veins generally hosing the sulfide mineralization in the form of mainly chalcopyrite and a lesser amount of bornite, galena and sphalerite while malachite, azurite and limonite/hematite occur as alteration/ leaching products.

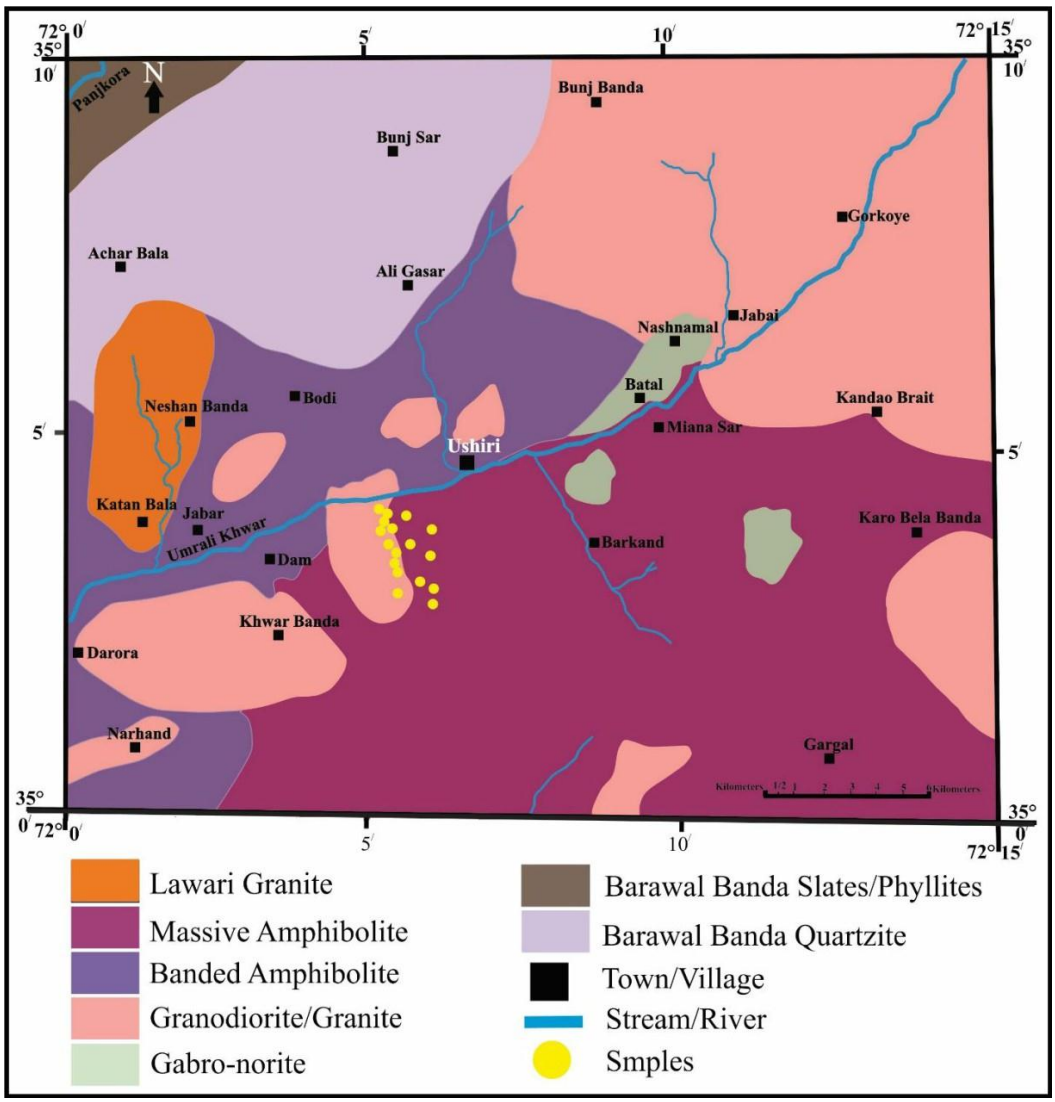

Fig. 2. The geological map of the study area modified after Haq et al. (2006), showing the locations of the samples

These mineralized quartz veins are generally associated with the shear zones where the sulfide mineralization is also found in dissemination in the host rocks adjacent to the quartz veins. The mineralized micro-veins following the foliation planes are also present which are probably the offshoots of the mineralized quartz veins. The quartz veins also contain clasts and pieces of the host rocks which have been incorporated in these veins during precipitation.

The mineralized host rocks, such as amphibolites, granodiorites and granites, found in association with the mineralized quartz veins along the shear zones have severe alteration where the hornblendes are altered to epidote and chlorite (i.e., propylitization), plagioclases are highly saussuritized and the alkali-feldspars exhibit severe alteration to kaolinite and sericite. In this respect, propylitization and silicification are the common features of the mineralized host rocks.

3. Materials and methods

During fieldwork, mineralized host rocks, alteration zones, mineralized quartz veins, and unmineralized host rocks were identified, and their field features were observed and photographed. Representative samples from the mineralized and unmineralized host rocks and mineralized quartz veins were collected. These collected samples were transported to the laboratory for experimental work at the National Centre of Excellence in Geology (NCEG), University of Peshawar.

Thin sections were prepared from mineralized and un-mineralized samples to study the petrographic features under the polarizing and reflecting microscope. The bulk and grab samples were crushed through a jaw crusher to small sizes (<1cm). About 200g of the crushed sample was extracted from each sample by passing it through the splitter. A representative crushed sample of about 50g was separated by quartering and conning. Subsequently, the crushed samples through the tungsten carbide mill were pulverized to a 200-mesh size for further geochemical analysis.

For major elements, a 0.5g sample was digested in hydrochloric, perchloric, and hydrofluoric acid to determine major oxides. A known amount of 1g of every sample was digested in aqua regia and hydrofluoric acid for the determination of trace elements, while for gold determination, 2g sample was digested in aqua regia and then gold was extracted in methyl isobutyl ketone (MIBK). The gold and major oxides were analyzed through a Perkin Elmer 700 series atomic absorption spectrometer. The Loss on Ignition (LOI) was obtained by igniting the sample overnight at 950°C.

For the analysis of trace and rare earth elements, 0.25g of finely powdered samples were taken in Teflon beakers and 3 ml of hydrofluoric acid (HF) and 2 ml of sulfuric acid ($H2SO_4$) were added. The samples were dried on a hot plate at low heat, followed by three successive additions of 3ml HF, with complete drying between each addition. Subsequently, 2ml of perchloric acid ($HClO_4$) was added. The trace elements were then recovered in 50 ml of purified 5% nitric acid (HNO_3). The samples were boiled for one hour, transferred into 250 ml beakers, and allowed to settle. After settling, 1 ml from each sample was taken and diluted to 1000 ml with 2% HNO_3. A blank sample was prepared using the same method, and the samples were analyzed using ICP-MS. All procedures were validated with certified reference materials and analytical-grade chemicals (Jenner et al., 1990; Chen et al., 2017).

For SEM/EDX studies special chips (1.5 x 1.5 cm) were prepared from altered/mineralized samples. These chips were finely polished, coated with carbon, and placed in the SEM chamber for analysis. For X-ray diffraction (XRD) analysis, representative mineralized rock powdered samples were placed in the sample holder. The XRD measurements were conducted using a Geol-X-Ray

Diffractometer under the following standard conditions: the two theta (θ) angle ranged from 5° to 80°, with a step size of 0.020° and a counting time of 1 second per step. The X-ray tube operated at a current of 40 mA and a voltage of 40 kV, with Cu Kα radiation (λ =1.5406 Å) as the target source. Peak intensities and D-spacing values were determined using the built-in software of the Geol. XRD system. All the analyses were carried out at various laboratories of the NCEG, University of Peshawar, except for oxygen and sulfur isotopes and XRD analysis, which were conducted at Pakistan Institute of Nuclear Sciences and Technology, Islamabad, and Centralized Resource Laboratory, University of Peshawar, respectively.

4. Results and Discussions

4.1. Sulfide mineralization

4.1.1 Field and visual observations

The mineralization in the study area has been identified in different forms such as 1) sulfide mineralization along quartz veins, 2) disseminated sulfide mineralization in the host rocks, and 3) supergene enrichment as leaching products of sulfide mineralization along shear zones. The polymetallic quartz veins have irregular medium to coarse-grained and micro veins of ore minerals mainly chalcopyrite, and pyrite with lesser amounts of bornite, galena, and sphalerite. Malachite, azurite, and limonite/hematite occur as alteration products of sulfide ore minerals. These quartz horizontal and sub-vertical. These veins represent symmetrical banded, vuggy quartz, comb texture, mosaic, massive sulfide ores with cavities and vugs (Figs. 3a-d). The disseminated ore grains dominantly of chalcopyrite and pyrite are noticed in the host rocks (i.e., amphibolites, granodiorites, and granites) (Figs. 3f, h, i). The chalcopyrite and pyrite occur as irregular medium to coarse- grained. The chalcopyrite grains are also found either crosscut vein or along fabric direction within the amphibolite (Figs. 3f, g). The alteration products of sulfides such as malachite, azurite, and limonite/hematite are usually leached out along the foliation planes as micro-veins, especially along localized faults and shear zones (Figs. 3a, b, g, h, i).

The paragenetic sequence of the various ore minerals (i.e., sulfides, oxides, and carbonates) can be divided into three main stages (Fig. 4) based on cross-cutting relationships through field observations, hand specimens, and microscopic study. These stages are the pre-ore stage, the main ore stage, and the post-ore stage. The pre-ore stage is dominated by the medium to coarse-grained, euhedral to sub-hederal pyrite and quartz. The main ore stage is defined by the fine to medium- and chalcopyrite, with minor amounts of bornite and galena. The post-ore stage is characterized by the assemblage of copper carbonates (malachite and azurite) and barren quartz and iron oxides (limonite/hematite). This stage is dominated by the replacement of chalcopyrite and bornite by malachite and azurite while the pyrite is replaced by limonite/hematite.

4.1.2 Ore Mineralogy

Chalcopyrite: Ore microscopic study shows that chalcopyrite, as strong yellow irregular grains, is the most abundant copper- bearing phase in both mineralized host rocks (i.e., amphibolite, granodiorite, and granite) and mineralized quartz veins. It occurs either as micro veins or disseminated irregular masses (framboidal) within the interstices of quartz and microfractures in the quartz veins or silicate phases within the mineralized host rocks. At places it is found in association with pyrite, limonite/hematite (Figs. 5a, d-e). The massive grains of chalcopyrite also have fracture-filled micro-veins of limonite/hematite (Figs. 5e, f). In some cases, the malachite and azurite replacement are so intense along margins and microfractures that the chalcopyrite is present as relics within the malachite and azurite mass (Fig. 5e). At places, the pyrite grains are also enclosed by chalcopyrite which is confirmed by the scanning electron microscope (SEM) images (Fig. 6).

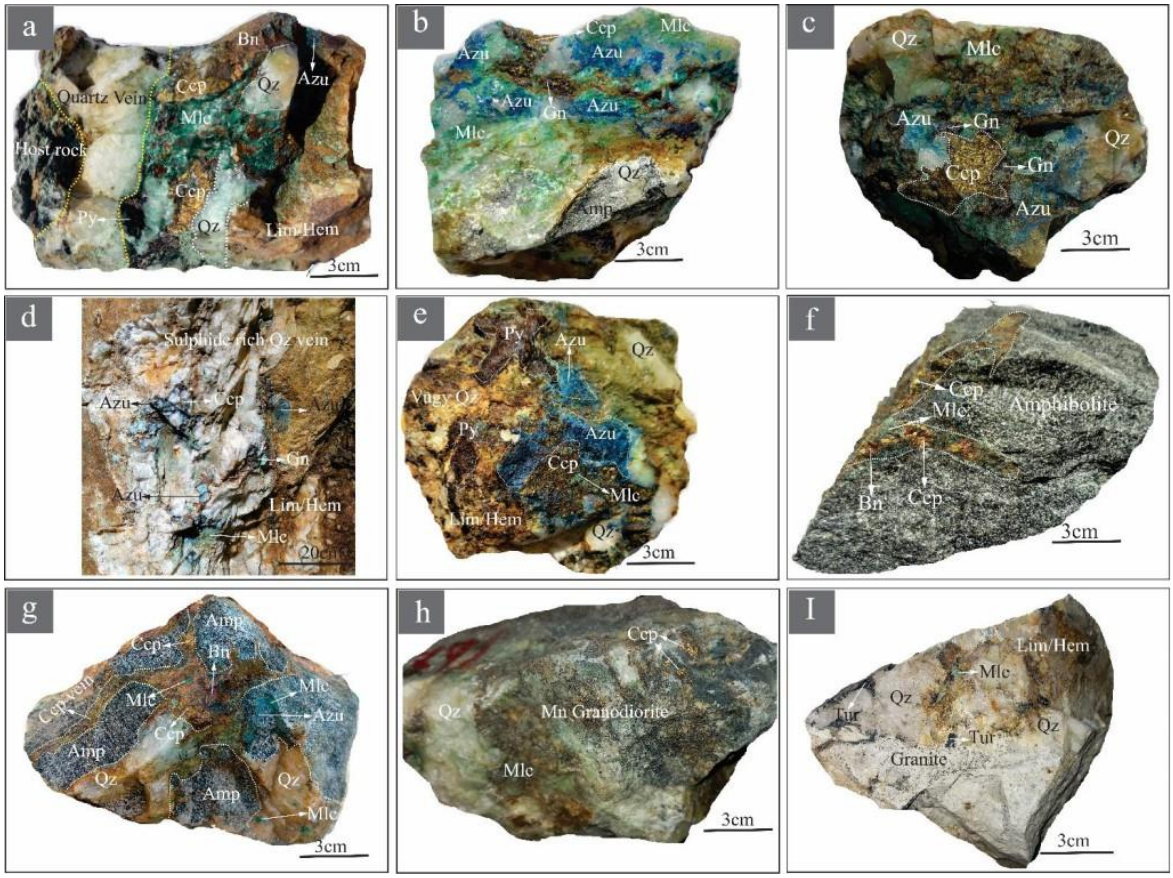

Fig. 3. Photographs of hand specimens illustrating metallic minerals in mineralized Quartz veins, amphibolites, granodiorites and granites: (a) mineralized host rock and mineralized quartz vein having bornite, azurite, malachite, chalcopyrite and limonite/hematite, (b) mineralized amphibolite and quartz having malachite, azurite, chalcopyrite and galena, (c) mineralized quartz contains massive grains of chalcopyrite, galena and azurite in disseminated form, (d)) mineralized quartz vein of azurite, malachite, galena and limonite/hematite, (e) ore body with pyrite, chalcopyrite, limonite/hematite and azurite, (f) amphibolite having chalcopyrite, bornite and malachite, which fabric of the rock, (g) amphibolite having veinlets of chalcopyrite and showings of malachite, bornite and azurite, (h) mineralized granodiorite comprising chalcopyrite, and malachite, (i) altered granite including quartz, malachite, and limonite/hematite. Abbreviations: Mlc=malachite, Azu=azurite, Py=pyrite, Ccp=chalcopyrite, Bn=bornite, Gn=galena, Hem=hematite, Mn=mineralized, Qz=quartz, Amp=amphibolite, after Whitney and Evans (2010).

Pyrite: Pyrite is the second abundant sulfide phase, occurring in both mineralized quartz veins and mineralized host rocks. In reflected light, it usually occurs as anhedral to euhedral light brass yellow medium-to coarse-grained, in association with chalcopyrite, sphalerite, and galena (Fig. 5c, d). In some cases, it is also enclosed in chalcopyrite. At places, the pyrite grains are usually fractured and these fractures are occasionally filled by limonite/hematite, whereas some irregular pyrite grains are also enclosed by limonite/hematite as relics (Figs. 5c, d). The euhedral, anhedral pyrite is confirmed by the SEM images (Fig. 6).

Bornite: Bornite as irregular grains occur in both mineralized quartz veins and mineralized host rocks in association with chalcopyrite. At places, it is found along the margins of chalcopyrite. In most cases, bornite is replaced by malachite and azurite.

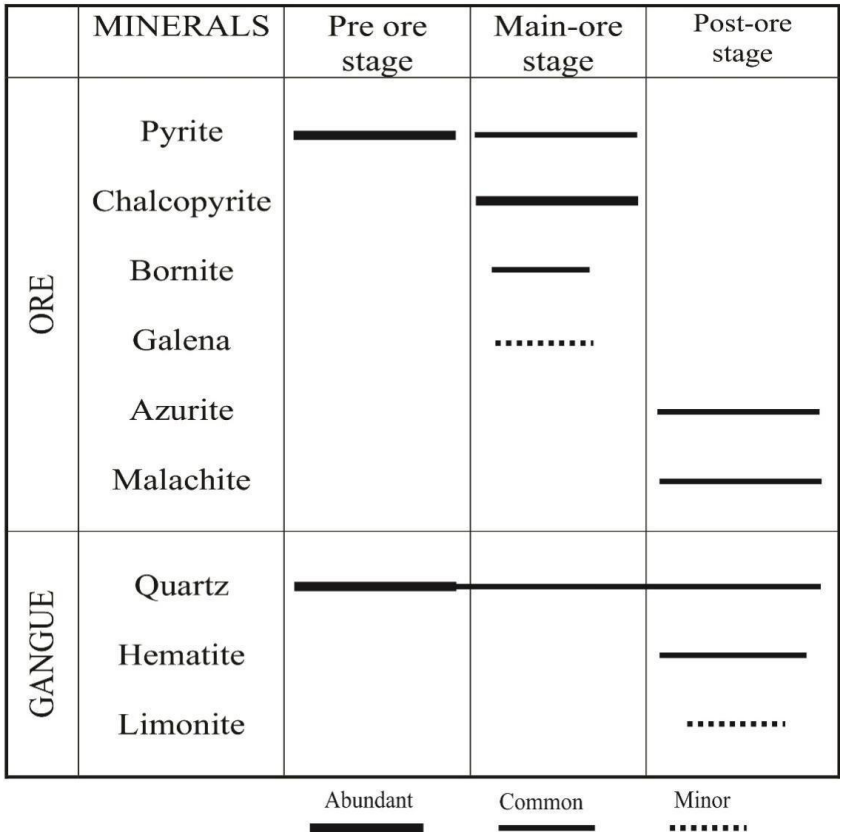

Fig. 4. Paragenetic sequence of the various ore minerals in the studied mineralization.

Sphalerite: Sphalerite, light gray to brown in color, occurs as an irregular medium to coarse-grained sulfide phase, usually inter-grown with chalcopyrite and galena (Fig. 5a). In some places, chalcopyrite grains are also enclosed in sphalerite.

Galena: Galena, silvery-gray in color, occurs in a minor amount as anhedral grains in mineralized quartz veins, usually found in association with chalcopyrite and pyrite (Figs. 5b, c). In some cases, it is inter-grown with chalcopyrite and pyrite and also contains limonite/hematite along the microfractures (Fig. 5d).

Malachite: Malachite occurs as green colored micro veins and irregular grains, associated with azurite, chalcopyrite, and hematite. It is the replacement product of chalcopyrite and bornite (Fig. 5e) which is generally found in the forms of micro-veins within the mineralized quartz veins and along the foliation planes within the mineralized host rocks.

Azurite: Azurite occurs as blue color micro-veins and irregular grains usually associated with chalcopyrite and bornite within the mineralized quartz veins and mineralized host rocks. It is the replacement product of mainly chalcopyrite and sometimes bornite along shearing zones.

Limonite/hematite: The limonite/hematite mixture is generally found in oxidized zones associated with supergene enrichment and is extensively spread throughout the mineralized quartz veins and mineralized rock either as micro-veins or irregular grains (Fig. 5). These phases usually occur as replacement products along fractures and margins of the sulfide phases, especially pyrite. In places of intense oxidation, these minerals have completely replaced the pre-existing sulfides.

The presence of all the ore minerals such as chalcopyrite, pyrite, sphalerite, galena and limonite/hematite have been confirmed by the XRD patterns in Fig. 7.

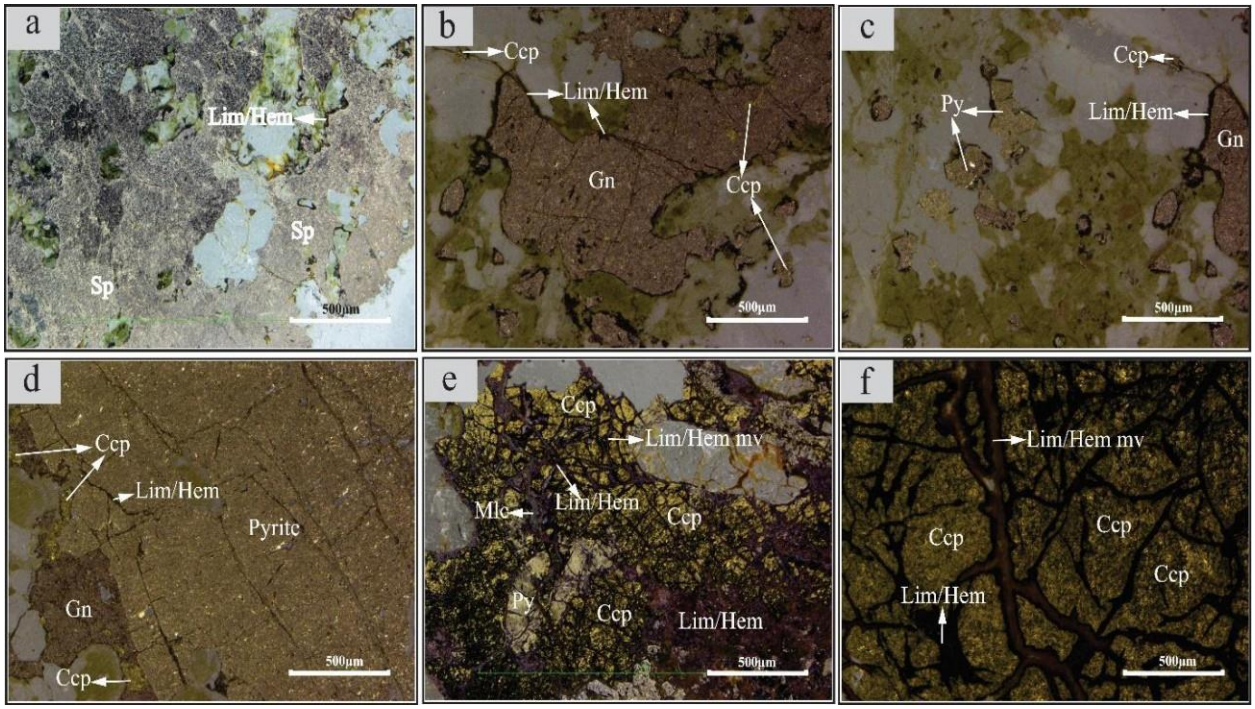

Fig. 5. Reflected light photomicrographs showing metallic minerals: (a) sphalerite and limonite/hematite are inter-grown in each other, (b) anhedral galena grains are inter-grown within the host rock, (c) limonite/hematite are formed along the massive galena grains. Some galena grains are also enclosed in the chalcopyrite, (d) galena, pyrite, limonite/hematite and chalcopyrite are found in association, (e) pyrite massive grain having limonite/hematite-filled fractures, (f) highly fractured chalcopyrite grains filled by limonite/hematite. The abbreviations are described in the caption to Fig. 3.

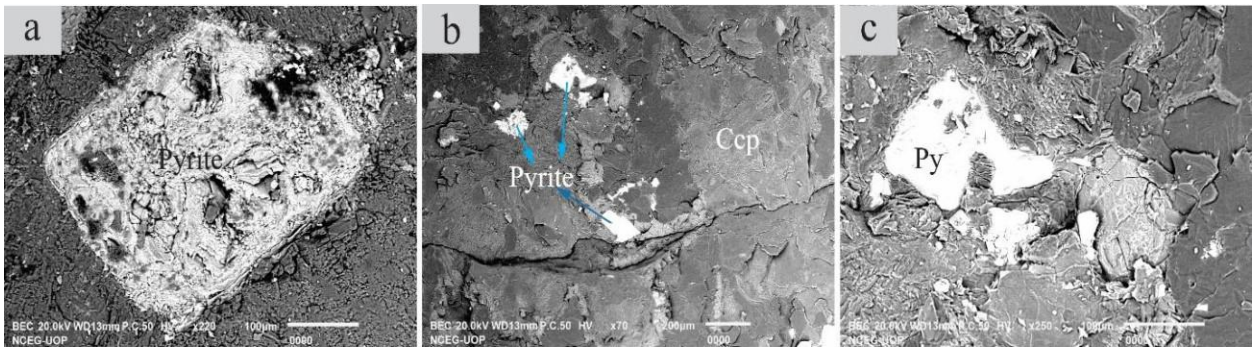

Fig. 6. The SEM backscattered images of selected mineralized quartz veins and mineralized host rock samples, showing the sulfides ore minerals. The abbreviations are described in the caption to Fig. 3.

The δ34S (VCDT ‰) values have been found as 0.93‰, 2.00‰, 1.40‰ and 4.40‰ in the, mineralized amphibolites, mineralized granodiorites, mineralized granites and mineralized quartz veins with an average amount of 2.18‰, respectively (Fig. 8a), while the δ18O (VSMOW) values have been found as 6.50‰, 7.20‰, 6.30‰ and 10.20‰ in the mineralized quartz veins, mineralized amphibolites, mineralized granodiorites and mineralized granites with an average amount of 7.50‰, respectively (Fig. 8b).

4.1.3 Hydrothermal alteration

The magmatic-hydrothermal alteration mostly consists of sericite-chlorite-epidote alteration assemblage (Sykora et al., 2018; Farhan et al., 2021; Hussain et al., 2023).

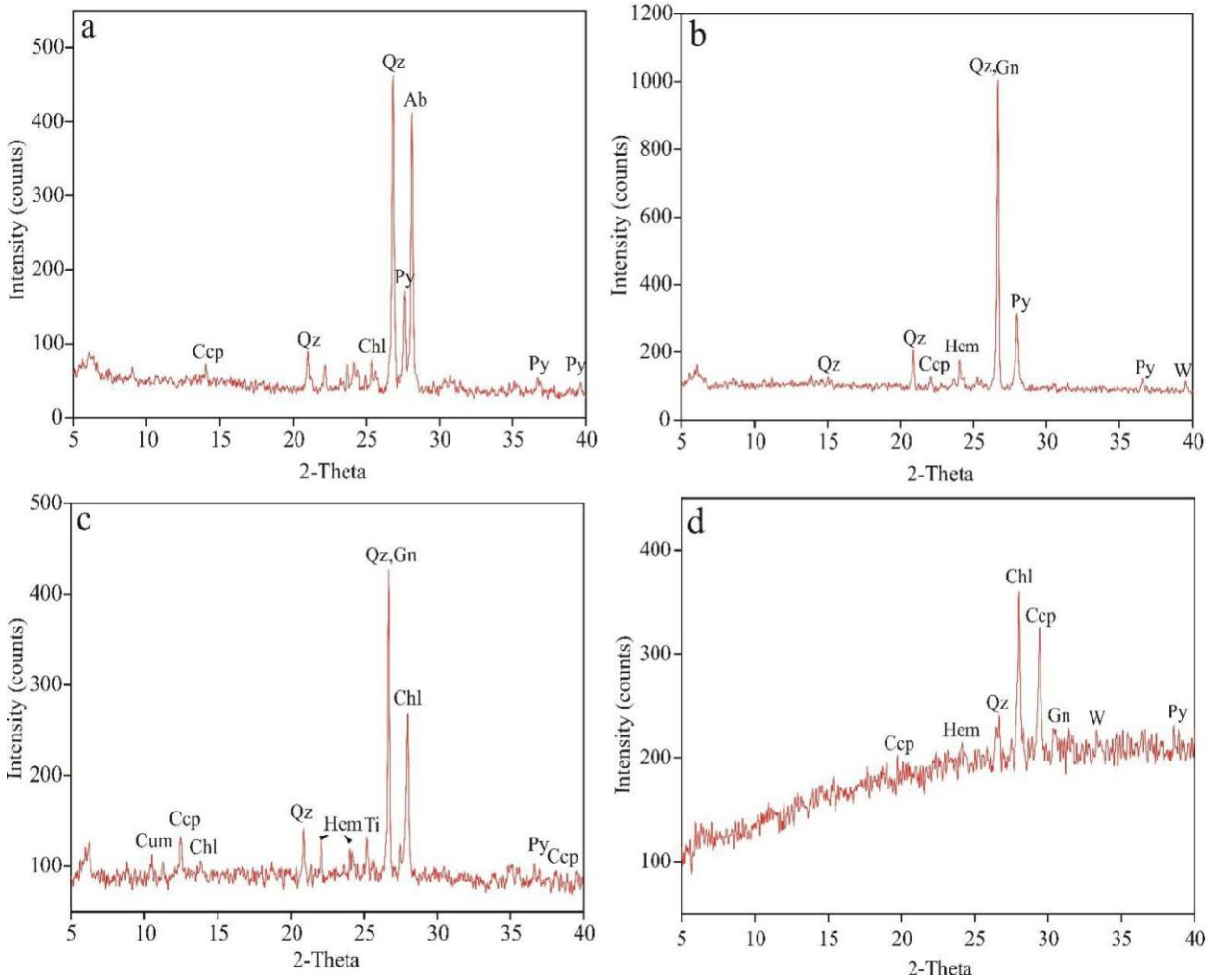

Fig. 7. XRD patterns of selected samples, showing the occurrences of various sulfide and oxide phases within (a) mineralized granites (b) mineralized granodiorites, (c) mineralized amphibolites and (d) mineralized quartz veins. Abbreviations: Py=pyrite, Ccp=chalcopyrite, Gn=galena, Hem=hematite, Qz=quartz, Ab=albite. Chl=chlorite, W=tungsten, Cum=cummingtonite, Ti=titanium.

This type of alteration is mostly associated with porphyry copper deposits, where the ore- forming fluids are magmatic in nature with a small amount of meteoric water (Simmons and Brown, 2006; Farhan et al., 2021; Hussain et al., 2023). In altered rocks the amphibole and feldspars are mostly dissolved by magmatic fluids, having greater amounts of HS, H2S, K+, Si, and low pH and HS (Liu et al., 2019; Hussain et al., 2023).

In the Ushiri Valley, the hydrothermal alterations are found within the sheared zones and at the contact zones of mineralized quartz veins and the host rocks. The alteration such as saussuritization, sericitization, Kaolinitization, Propylitization, and silicification in the mineralized host rocks are mainly formed due to the wall rock and hydrothermal fluid interaction. These alteration types support the mineralization characteristics of the study area similar to porphyry-style deposits. Sericitization and Kaolinization, mainly caused due to the alteration of alkali-feldspar in the studied mineralized host rocks, consist of quartz, kaolinite and sericite with a minor amount of biotite and muscovite, in contact with main sulfide ores. Saussuritization, mainly caused due to the alteration of plagioclase in the mineralized host rocks, is so intense that the plagioclase is partially or completely replaced by saussurite.

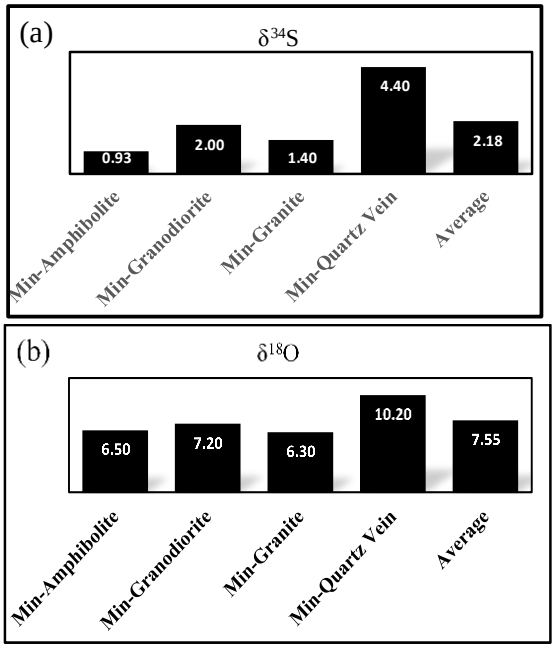

Fig. 8. Histogram showing the results of b34S and .5180 in ‰ in the mineralized/altered host rocks and mineralized Quartz veins from the study area.

The chlorite and epidote are frequently replacing the plagioclase and hornblende in the mineralized host rocks. In the altered host rocks, the sericite and propylitic (chlorite-epidote) alterations are mostly formed by slightly hydrothermal fluid acidic in nature, at temperatures between 200-300 ˚C and 200-400 ˚C (Sykora et al., 2018; Liu et al., 2019; Hussain et al., 2023). The silicification in the studied mineralized host rocks is composed of fine to medium-grained subhedral to anhedral, massive and vuggy quartz. It is closely associated with mineralization and is observed across the pre-ore stage and post-ore stage. The silicification usually occurs at low, moderate, and high temperatures associated with Au-Zn-Cu-Pb-U, and Mo-Sn-W, Cu-Pb mineralization (Zhu et al., 2006; Hussain et al., 2023). In the study area, the alteration minerals assemblages (sericite, kaolinite, saussurite, chlorite-epidote, and silica) show a strong similarity with the worldwide various deposits types, such as Mirkhani Cu-Au, Kargah vein type deposit, Axi ore deposit, and Bubin Cu-Pb deposit which were formed in the temperature range of 215-322˚C, 313-555˚C, > 285˚C, and 154-540˚C, respectively, indicating that they are hydrothermal in nature (Zhai et al., 2019; Farhan et al., 2021; Hussain et al., 2021).

4.1.4. Mass transfer accompanying alteration and mineralization process

The interaction of hydrothermal fluids with the surrounding rocks during the hydrothermal alteration process changes the physical and chemical characteristics of rocks. It results in the formation of new minerals under a suitable geological environment, as the hydrothermal fluids may remove or add certain elements to the host rocks. Several methods have been adopted for the calculation of chemical change in the form of losses and gains of certain elements for mineralized/altered rocks, however, the isocon method has been chosen as the preferred method of calculation (Gresens, 1967; Grant, 1986).

The isocon equation is essential and widely adopted as it calculates the changes in concentration, mass, and volume of host rocks and their mineralized counterparts (Trincal et al, 2014; Geo et al., 2017; Farhan et al., 2021). The isocon is a straight line showing the immobile elements on a graph (Fig. 9) near or along this line, with unmineralized rocks on the x-axis plotted against the mineralized rocks on the y-axis. This line separates the enriched, depleted, and immobile elements. The enriched elements are plotted above the isocon line, the depleted elements below the isocon line, and the immobile on or near the isocon line. The equation for this method based on Gresen's equation (Gresens, 1967; Grant, 1986) is as follows:

$$\Delta Ci = M^A/M^O\ (C_I^A - C_I^O) \quad \text{..... (1)}$$

Where M^A and M^O are masses of altered and corresponding unaltered rock, respectively (M = Vp, V = volume, and p = density), C_I^A and C_I^O are the element concentrations ‘i’ in altered/ least and altered rock. Equation (1) can also be written as;

$$C_I^A = M^O/M^A\ (C_I^o + \Delta Ci) \quad \text{..... (2)}$$

Table 1: Chemical analysis of unmineralized, mineralized host rocks and mineralized quartz veins for major oxides (%), trace and rare earth elements (ppm).

	Unmineralized rocks							Mineralized host rocks and quartz veins									
	Granodiorites		Granites			Amphibolites		Granodiorites		Granites			Amphibolites		Quartz veins		
Sample	U1A	U2A	U3A	U5A	U8A	U6A	U7A	U1B	U2B	U3B	U5B	U8B	U7B	U9	U4	U6B	U10
SiO_2	64.2	64.3	72.1	74.2	71.4	51.1	50.2	52.02	45.01	64.02	66.06	68.4	43.3	41.02	58.1	64	66.01
TiO_2	0.5	0.42	0.2	0.1	0.3	0.6	0.9	0.5	0.42	0.2	0.1	0.6	0.6	0.9	0.22	0.4	0.21
Al_2O_3	14.1	14.2	14.1	12.6	14.2	17.2	16.8	14.1	14.2	14.1	12.5	14.2	17.2	16.8	3.2	4.2	4.1
FeOt	6.1	6.3	2.3	2.1	2.4	9.6	9.4	19.12	28.1	9.01	8.03	5.4	17.02	16.01	25.1	17.05	17.2
MnO	0.07	0.06	0.1	0.1	0.2	0.13	0.15	0.1	0.02	0.08	0.02	0.1	0.01	0.02	0.13	0.16	0.12
MgO	2.1	2.2	0.5	0.4	0.6	6.6	7.2	1.2	0.31	0.36	0.21	0.4	3.018	4.2	0.6	0.93	0.5
CaO	4.8	5.02	2.6	2.8	2.5	8.2	9.3	3.8	2.50	2.5	2.15	2.4	5.04	6.2	0.6	1.28	0.7
Na_2O	2.9	3.1	4.1	3.2	3.8	2.9	2.1	1.4	1.25	2.15	2.16	2.2	1.4	1.02	1.02	1.22	1.01
K_2O	2.7	2.6	2.5	2.1	2.4	0.81	0.82	3.6	4.04	3.3	3.14	2	3.2	3.5	0.26	0.21	0.25
P_2O_5	0.1	0.08	0.18	0.12	0.1	0.23	0.12	0.2	0.01	0.1	0.14	0.1	0.02	0.03	0.1	0.12	0.1
CuO	---	---	---	---	---	---	---	1.53	2.41	2.04	3.53	2.27	5.79	7.29	8.21	7.32	7.33
LOI	1.4	1.3	0.8	1.02	0.9	1.5	1.3	1.2	0.62	0.8	0.91	0.9	2	1.6	0.92	1.15	1.1
Total	98.97	99.58	99.48	98.74	98.8	98.87	98.29	98.8	98.9	98.6	98.9	98.9	98.60	98.6	98.5	98.04	98.6
V	112	121	34	36	22	262	248	20	90	16	19	18	56	65	24	10	21
Cr	32	40	50	32	42	8	13	92	122	84	130	72	38	53	36	25	35
Ni	18	22	8	7	12	122	145	72	80	34	62	20	210	198	82	80	56
Cu	17	14	30	10	22	72	80	12302	19328	16356	28256	18222	46348	58332	65702	58612	58703
Zn	14	12	34	28	50	40	62	210	1821.1	4037.7	4186.6	52	212	231	256	0	132
Rb	68	58	72	122	83	14	18	48	90.1	61	53	56	12	10	21	22	20
Sr	290	272	180	210	190	90	98	80	121	89	113	72	70	61	88	82	90
Zr	12.3	12.2	10.3	8.8	10	23	24	11.8	12	10	8.6	9	20	22	3	2	2
Y	21	20	18	24	20	14	21	302	1204	16	13	12	38	41	10	21	8
Pb	4	7	42	20	50	4	3	316	2258	2142	3142	112	231	312	602	312	512
Sb	0.3	0.2	0.5	1	1	1	0.5	5	6	4	6	2	2	3	7	7	5
Co	9	10	48	56	30	52	46	93	120	118	82	112	65	73	12	7	5
Mo	0.8	0.7	3	1	2	0	0	2	1	2	1	1	0.11	0.12	1	3	1
W	2	1	1	0.5	1	0	0	30	2786.3	1690.3	1502.9	21	5	6	230	32	48
Ag	<0.05	<0.05	<0.05	<0.05	<0.05	<0.05	<0.05	2	51.4	79.5	988.6	6	<0.05	<0.05	6	6	3
Th	10	9	7	6	8	0.2	0.3	5	5	6	5	6	0.4	0.2	0.21	0.32	0.31
Ce	42	30	21	28	20	8.2	9.4	15	12	13	12	17	8	7	13	12	11
Pr	4.8	5.2	3	5	2	1.3	1.2	4	4	3	2	1	1.2	1	1	0.8	1
Nd	22.7	15.3	8	9	10	7.4	8.1	6	10	7	5	9	6	5	2	0.8	2
Sm	3.6	4.2	3	1	2	3.1	2.6	1	2	1	2	1	3	2	1	0.7	1
Eu	1	1	2	1	1	0.92	0.88	1	1	1	1	1	0.7	0.8	0.62	0.6	0.5
Gd	3.2	2.9	1	2	2	2.4	2.3	2	2	2	1	2	2	1	1	5	1
Tb	0.6	0.7	1	2	1	0.62	0.58	1	0.3	1	1	1	0.4	0.5	0.2	0.36	0.21
Au	<0.05	<0.05	<0.05	<0.05	<0.05	<0.05	<0.05	<0.5	<0.05	<0.05	<0.05	<0.05	<0.05	<0.05	3	4	4
Dy	5	4	1	2	2	3.2	2.8	1	3	1	1	1	2	2	1.92	1.6	2.1
Ho	0.6	0.8	1	1	1	0.8	0.9	0.5	0.5	0.3	1	0.5	0.6	0.7	0.13	0.11	0.12
Tm	0.6	0.5	1	1	1	0.4	0.3	0.8	0.4	0.6	1	0.7	0.2	0.2	0.3	0.31	0.2
Yb	3	2	1	1	1	1.8	2	1.02	1	1	1	0.8	1	2	0.6	0.42	0.7
Lu	0.42	0.4	0.5	1	1	0.4	0.41	9	0.3	0.4	0.5	0.8	0.3	0.4	0.13	0.41	0.12
As	3.5	3.2	8	16	12	0.1	0.1	4	3	5	12	11	0.01	0.02	0.03	0.03	0.04

Where Ci (concentration of elements) O and A superscripts represent the unmineralized and mineralized rock. ΔCi shows the change in the concentration of an element. The isocon is obtained by plotting the unmineralized rocks on the x-axis, while the mineralized rocks are plotted on the y-axis. The immobile elements have no loss or gain ΔCi = 0, the equation becomes;

$$C^A = (M^O/M^A)C^O . \quad ..... (3)$$

For each sample, the volume change can be obtained through rock density values and (M^A/M^O) ratio corresponding to the isocon:

$$\Delta V = (V^A/V^O) = (M^A/M^O) * (\rho^A/\rho^O) \quad .....(4)$$

The gains and losses of major and trace elements as well as volume change (ΔV) are calculated from Gresen's equation (Gresens, 1967).

In order to calculate the mass transfer during the alteration/mineralization process in the study area, the major and trace elements of the studied unmineralized rocks, mineralized rocks and mineralized quartz veins, as given in Table 1, were plotted in the Isocron diagram (Fig. 9). The unmineralized rocks were plotted on the X-axis against the mineralized rocks on the Y-axis in the form of scattered plots to obtain the losses and gains of components for the representative studied samples (Fig. 9).

In the mineralized granites, among the major oxides, SiO_2 and Na_2O are depleted, while the FeO and K_2O are highly enriched with a slight increase in MgO, CaO, and P_2O_5. The Al_2O_3 and TiO_2, are the isocon elements, i.e., their concentrations remain unchanged (Fig. 9a). Among the trace elements, the highly enriched elements are Cu, Pb, Zn, and W, while the slightly enriched ones are Cr, Ni, and Co (Fig. 9 a). The depleted trace elements are V, Rb, Ce, Sr, and Nd. The volume loss is -5.56% during mass transfer and alteration.

In the mineralized granodiorites, among the major oxides, SiO_2, Na_2O, MnO, MgO, CaO, and P_2O_5 are depleted, FeO and K_2O are enriched, and Al_2O_3 remains unchanged. Among the trace elements, the highly enriched elements include Cu, Pb, Zn, and W, while the depleted elements are Sr, Rb, Y, and Ce (Fig. 9b). In granodiorites during alteration/mineralization, the volume gains of 33.2% occurred during the mass transfer.

In the mineralized amphibolites, the MgO, CaO, Na_2O and SiO_2, are depleted, whereas slight depletion in P_2O_5 and MnO are noticed. The TiO_2 and Al_2O_3 remain unchanged and K_2O and FeO are enriched. Among the trace elements, Cu and Pb are highly enriched, while Zn, Ni, and Co are slightly enriched, and depleted trace elements are V, Sr, Zr, and Y (Fig. 9c).

The volume loss 11.48% occurred during mass exchange and hydrothermal alteration. In mineralized quartz veins relative to amphibolites, the SiO_2, and FeOt are highly enriched while the rest of the major oxides are depleted. In trace elements, the Cu and Pb are highly enriched (Fig. 9d).

In conclusion, the results from our elemental gain and loss calculations provide a significant insight into the mineralization processes occurring within the ore deposits. Our analysis indicates that the ore-forming fluids were significantly enriched in FeO, K_2O, Cu, Pb, Zn, W, Cr, Ni, and Co in granite, FeO, K_2O, Cu, Pb, Zn, and W in granodiorite, FeO, K_2O, Cu, Pb in amphibolite and quartz veins, suggesting a substantial influx of these elements during mineralization. These enrichments are indicative of the complex geochemical interactions between the mineralizing fluids and various host rocks, highlighting the importance of understanding these processes for better exploration and exploitation of ore deposits. In all the samples, the concentration of Cu is extremely high, suggesting the hydrothermal fluids were Cu-rich.

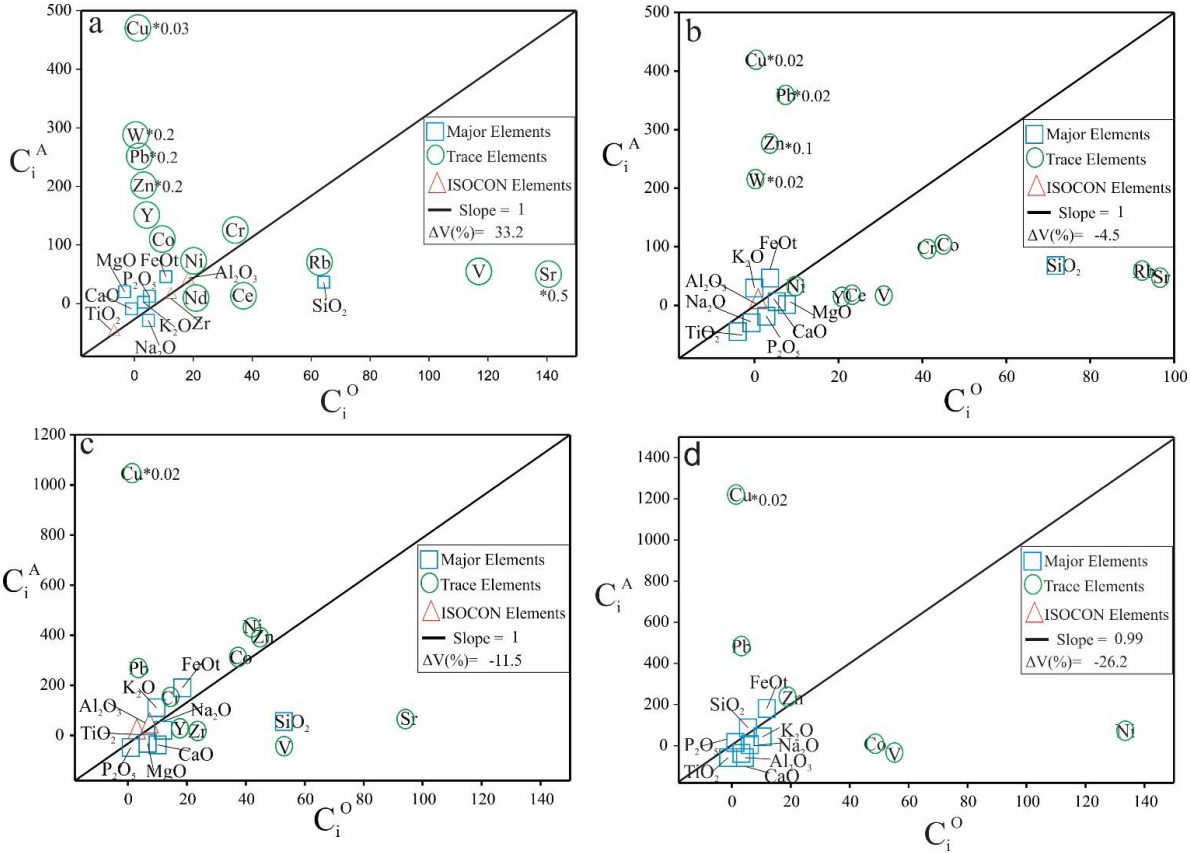

Fig. 9. Isocon diagrams for (a) granite, (b) granodiorite, (c) amphibolite, and (d) quartz veins, major oxides in %, trace elements in ppm show the enriched elements above the isocon line, while depleted elements below, and the unchanged elements on the isocon line. Abbreviations: C_i^o = element contents in unmineralized rock; C_i^A = element contents in mineralized rock.

The concentrations of K, Zn, Ni, and Cr are high in mineralized samples, implying the hydrothermal fluids might be derived from the mantle/magmatic source. On the other hand, the observed depletion of certain elements in the mineralized rocks suggests selective leaching or mobilization during mineralization. These findings emphasize the dynamic nature of ore-forming environments.

4.1.5. Source of the ore-forming Fluids

Oxygen and sulfur isotopes play a crucial role in solving the complex processes involved in the formation of ore deposits, contributing important insights into their genesis and evolution. In the formation of ore deposits, the minerals isotopic compositions indicate crucial information about the characteristics and sources of ore-forming fluids, as well as redox conditions and dominant temperature during mineral deposition (Ohmoto, 1987; Hofstra et al., 2001; Seal, 2006). The sulfur isotopes define the oxidation-reduction conditions of involved fluids and sources of the metals, while the oxygen isotopes illuminate the temperature at which fluids interaction occurred with host rock and delineate the origin of hydrothermal fluids (Gena et al., 2006; Le et al., 2022). Furthermore, isotopic analysis explains the hydrothermal alteration processes, and fluids mixing within the ore-forming systems, revealing the pathways and mechanism of the vibrant mineral deposit formation (Candela and Holland, 1986; William-Jones and Migdisov, 2014).

The sulfur isotope ($\delta^{34}S$) in the sulfide-rich host rocks (i.e., amphibolite, granodiorite and granite) of the study area ranges from 0.93‰ to 4.4‰, with an average of 2.18 ‰ which is almost consistent with the majority of the world's

magmatic-hydrothermal deposits having $\delta^{34}S$ as 0±3‰ (Ohmoto, 1979, 1987). The previous studies infer that the sulfur isotopic composition in sulfide minerals depends on the hydrothermal fluids evolution, physicochemical conditions, and the $\delta^{34}S$ source materials (Li et al., 2018; Gao et al., 2020). The variation of $\delta^{34}S$ in magmatic-hydrothermal deposits is due to the assimilation of sulfur from the wall rocks, the contamination of magma with country rocks and the boiling process during mineralization (Hoefs, 2009; Kendall et al., 2009). In the study area, the hydrothermal wall rock alteration is mostly present in the mineralized host rocks found at the contact zone with the quartz-bearing sulfide veins and also within the localized sheared zones. In this respect, the average $\delta^{34}S$ value of 2.18‰ of the studied mineralized host rocks suggests magmatic and deep mantle sources for the mineralizing fluids whereby the sulfur was transported from deep-seated magma through fluid input and contamination of sulfur from the host rock.

The most distinct feature of oxygen isotopic data from the rocks of the study area is the $\delta^{18}O$ enrichment in the mineralized rocks and the mineralized quartz veins. The previous studies suggest that the $\delta^{18}O$ values from 5.5‰ to 9.5‰ are typical magmatic water or magmatic fluid (Ohmoto, 1979, 1987). In this respect, the higher oxygen isotopic signature (i.e., 6.50‰ to 10.20‰ with an average value of 7.55‰) of both the mineralized rocks and the mineralized quartz veins has ruled out the involvement of meteoric water and suggests some kind of heavy fluid comparable to magmatic fluid is responsible for the alteration and sulfide mineralization in the studied rocks.

4.1.6. Genesis of the sulfide mineralization

Most of the magmatic-hydrothermal ore deposits are associated with the island arc tectonic setup and are usually linked to subduction-related magma (Sillitoe, 2010; Hussain et al., 2023). The Ushiri valley amphibolites as part of the Kamila amphibolites, granodiorites and granite as part of the Kohistan batholith in the westernmost part of the Kohistan island arc also originated by the subduction-related magma. Therefore, it can be postulated that the magmatic-hydrothermal fluids having the ability to form complexes with the metals, can be responsible for the ore metal transporting agent in these rocks. Due to the involvement of heavy liquid, it can be hypothesized that the intrusive bodies of some sort may have existed underneath these rocks which could have been the source of high-temperature metalliferous fluids which could have been magmatic water exsolved from these intrusions. Such fluids are of great importance in porphyry copper deposits (Sheppard et al., 1976; Harris et al., 2005; Wilson et al., 2007; Sun et al., 2024).

The magmatic-hydrothermal model is supported by the existence of ore/metallic mineralization occurs in fracture and vein fillings, as well as disseminated ore grains in the form of chalcopyrite, bornite, sphalerite and galena. Intergrown textures among these sulfides suggest simultaneous crystallization from hydrothermal fluids with early crystallization of the copper-rich phase (i.e., chalcopyrite). These ore phases mostly show mutual grain contact and linear sharp boundaries. The fracture-filling and micro vein nature of these sulfides, especially chalcopyrite, represent hydrothermal fluids activity. The replacement of early-formed ore minerals by new minerals and wall rock alterations such as sericitization, kaolinization, silicification, and propylitization also favor the hydrothermal environment/features (Liu et al., 2019; Zhai et al., 2019).

Moreover, in Ushiri Valley, the $\delta^{34}S$ and $\delta^{18}O$ values strongly resemble most of the worldwide magmatic-hydrothermal deposits. The sulfur isotopic data is in conformity with most of the world's magmatic ore deposits (Fig. 10) such as the

Cu-Au deposit in Shizishan, Anhui, China (Xia et al., 2002), the porphyry copper deposit, Cadia, southeastern Australia (Wilson et al., 2007), Axi ore deposit (Zhai et al., 2009), Yinan Au-Cu-Fe deposit (Zhang et al., 2011), Shagou Ag-Pb-Zn deposit (Han et al., 2014), Shurab Sb-polymetallic vein deposit, eastern Iran (Mehrabi et al., 2019), Jinchang, Gold-Copper deposit in Heilongjiang Province, Northeastern China (Li et al., 2019), Kargah polymetallic vein-type deposit (Hussain et al., 2012), Mirkhani Cu-Au (Farhan et al., 2021), and Bubin polymetallic deposit (Hussain et al., 2023).

The oxygen isotope data are also consistent with the porphyry deposit in Bingham, Utah (Roedder, 1971), Ann-Mason Porphyry Copper Deposit, Yerington, Nevada (Dilles et al., 1992), El Salvador porphyry copper deposit, Chile (Sheppard and Gustafson, 1976), Babine porphyry Cu deposits, British Columbia (Zaluski et al., 1994), Bajo de la Alumbrera Copper-Gold deposit (Harris et al., 2005), Yaoling vein-type polymetallic deposit in South China (Yang et al., 2019), the super-giant Grasberg porphyry Cu-deposit in Indonesia (Mernagh et al., 2020), and Zhunuo porphyry Cu deposit, China (Sun et al., 2024).

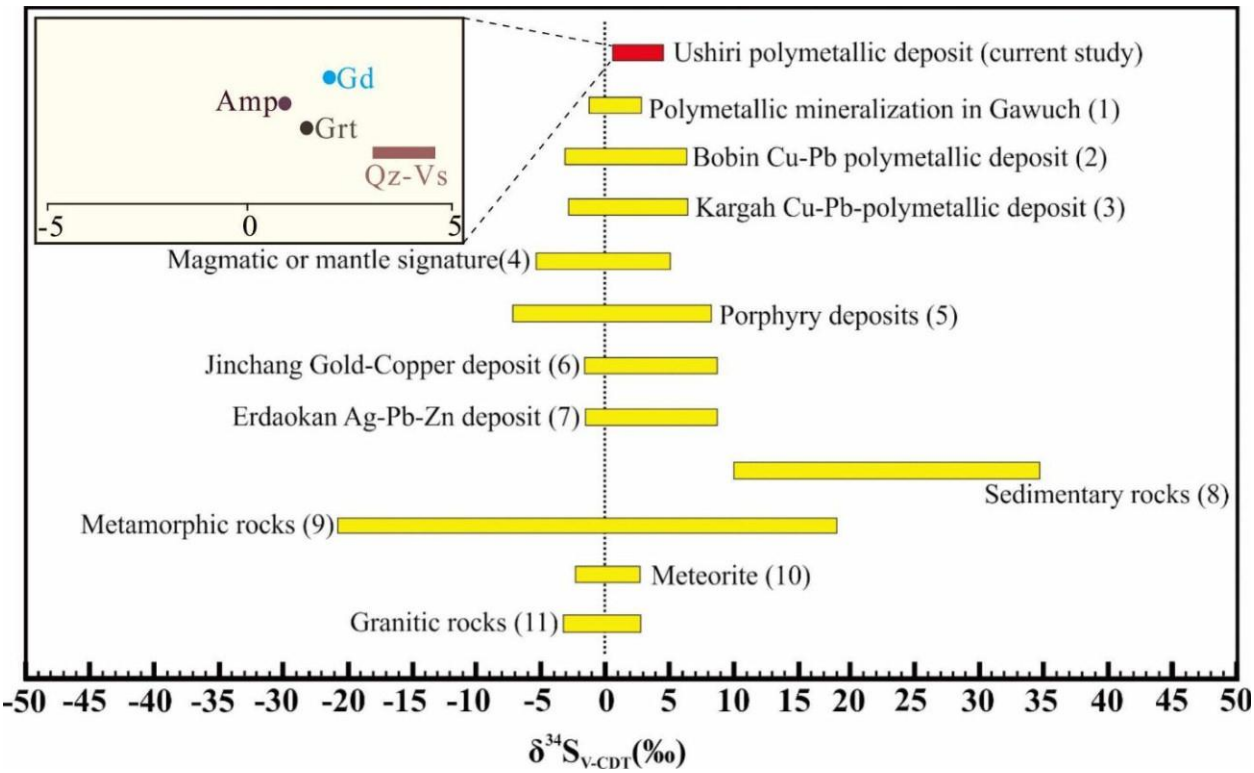

Fig. 10. Comparison of the range of $\delta^{34}S$ values of the Ushiri Valley minerals deposit with sulfur isotopic compositions of different geological materials. Data sources, (1) Farhan et al. (2023), (2) Hussain et al. (2023), (3) Hussain et al. (2021), (4) Yuan et al. (2019), (5) Ohmoto (1979), (6) Li et al. (2019), (7,8,9) Yuan et al. (2019), (10) Rollinson (1993), (11) Seal (2006).

5. Conclusions

- Various types of rocks (i.e., amphibolites, granodiorite and granites) of the Ushiri valley have three types of mineralization such as 1) sulfide mineralization along quartz veins, 2) disseminated sulfide mineralization in the host rocks, and 3) supergene enrichment of mineralization along localized shear zones.
- Chalcopyrite is the dominant copper-bearing sulfide phase with a subordinate amount of bornite, sphalerite and galena as the primary phases in both mineralized host rocks and mineralized quartz veins. The supergene enrichment in the form of

malachite, azurite and limonite/hematite is the characteristic feature of localized shear zones.

- The sulfide mineralization precipitated in three different stages; the pre-ore stage is dominated by pyrite, the main-ore stage consists of pyrite, chalcopyrite, bornite, galena, and sphalerite, while the post-ore stage contains the replacement minerals such as malachite, azurite and limonite/hematite.
- The mineralized host rocks exhibit severe alteration in the form of saussuritization, sericitization, kaolinization, propylitization, and silicification which is caused by the hydrothermal fluid related to porphyry-type deposits.
- The enrichment and depletion calculations show that the ore-forming fluids were significantly enriched in FeO, K_2O, and Cu, while the Pb, Zn, W, Cr, Ni, and Co were slightly enriched.
- On the basis of sulfur and oxygen isotopic data, it is suggested that some sort of heavy fluid of magmatic origin related to the intrusive bodies at depth is responsible for the precipitation of mineralized quartz veins and associated mineralized host rocks at the contact zones and along the weak/shear zones in the study area.

Author's Contribution

Israr Ud Din: Conceptualization, Sampling, Methodology, software, formal analysis, visualization, Validation, Writing-Original draft preparation. Asghar Ali: Conceptualization, Sampling, Methodology, formal analysis, writing review and editing. M. Tahir Shah: methodology, writing review and editing, supervision. Muhammad Farhan: methodology, validation, writing review, and editing.

Acknowledgment

This paper is a part of the PhD research of Mr. Israr Ud Din. The authors express their gratitude to the National Centre of Excellence in Geology, University of Peshawar, for providing the necessary fieldwork and laboratory facilities.

References

Alam, M., Li, S. R., Santosh, M., Shah, A., Yuan, M. W., Khan, H., & Zeng, Y. J. (2019). Morphological, thermos-electrical, geochemical and isotopic anatomy of auriferous pyrite from the Bagrote Valley placer deposits, North Pakistan: Implications for ore genesis and gold exploration. *Ore Geology Reviews, 112*, 103008. https://doi.org/10.1016/j.oregeorev.2019.103008

Ali, L. (2011). *Gold and base metal exploration studies based on mineralogical and geochemical characterization of stream sediments from North Pakistan* (Doctoral dissertation, University of Exeter, United Kingdom).

Bignold, S. M., & Treloar, P. J. (2003). Northward subduction of the Indian Plate beneath the Kohistan island arc, Pakistan Himalaya: New evidence from isotopic data. *Journal of the Geological Society, 160*(3), 377–384. https://doi.org/10.1144/0016-764902-154

Bignold, S. M., Treloar, P. J., & Petford, N. (2006). Changing sources of magma generation beneath intra-oceanic island arcs: An insight from the juvenile Kohistan island arc, Pakistan Himalaya. *Chemical Geology, 233*(1–2), 46–74. https://doi.org/10.1016/j.chemgeo.2006.03.008

Brown, D., Ryan, P. D., Herrington, R. J., & Brown, D. (2011). The generation and preservation of mineral deposits in arc–continent collision environments. In *Arc–continent collision* (pp. 145–159).

Candela, P. A., & Holland, H. D. (1986). A mass transfer model for copper and molybdenum in magmatic hydrothermal systems: The origin of porphyry-type ore deposits. *Economic Geology, 81*(1), 1–19. https://doi.org/10.2113/gsecongeo.81.1.1

Chen, S., Wang, X., Niu, Y., Sun, P., Duan, M., Xiao, Y., & Xue, Q. (2017). Simple and cost-effective methods for precise analysis of trace element abundances in geological materials with ICP-MS. *Science Bulletin, 62*(4), 277–289. https://doi.org/10.1016/j.scib.2016.12.012

Coward, M. P., Butler, R. W. H., Khan, M. A., & Knipe, R. J. (1987). The tectonic history of Kohistan and its implications for Himalayan structure. *Journal of the Geological Society, 144*(3), 377–391. https://doi.org/10.1144/gsjgs.144.3.0377

Dilles, J. H., Solomon, G. C., Taylor, H. P., & Einaudi, M. T. (1992). Oxygen and hydrogen isotope characteristics of hydrothermal alteration at the Ann-Mason porphyry copper deposit, Yerington, Nevada. *Economic Geology, 87*(1), 44–63. https://doi.org/10.2113/gsecongeo.87.1.44

Farhan, M., Arif, M., Ye, Y., Li, C. F., Chen, X., Garbe-Schönberg, D., & Khan, A. (2023). Fluid source and physicochemical conditions of the polymetallic mineralization in Gawuch Formation, Kohistan Island Arc, NW Pakistan. *Geochemistry, 83*(1), 125949. https://doi.org/10.1016/j.chemer.2022.125949

Farhan, M., Arif, M., Ying, Y., Chen, X., Garbe-Schönberg, D., Ullah, Z., & Li, C. F. (2021). Host rock peculiarities and influence of major structures on gold and base metal sulfide mineralization in northern Pakistan. *Periodico di Mineralogia*, *90*(1), 137–171.

Gao, R., Xue, C., Chi, G., Dai, J., Dong, C., Zhao, X., & Man, R. (2020). Genesis of the giant Caixiashan Zn–Pb deposit in Eastern Tianshan, NW China: Constraints from geology, geochronology and S–Pb isotopic geochemistry. *Ore Geology Reviews, 119*, 103366. https://doi.org/10.1016/j.oregeorev.2020.103366

Gao, R., Xue, C., Lü, X., Zhao, X., Yang, Y., & Li, C. (2017). Genesis of the Zhengguang gold deposit in the Duobaoshan ore field, Heilongjiang Province, NE China: Constraints from geology, geochronology and S–Pb isotopic compositions. *Ore Geology Reviews, 84*, 202–217. https://doi.org/10.1016/j.oregeorev.2017.01.015

Gena, K. R., Chiba, H., Mizuta, T., & Matsubaya, O. (2006). Hydrogen, oxygen and sulfur isotope studies of seafloor hydrothermal system at the Desmos caldera, Manus back-arc basin, Papua New Guinea: An analogue of terrestrial acid hot crater-lake. *Resource Geology, 56*(2), 183–190. https://doi.org/10.1111/j.1751-3928.2006.tb00273.x

Grant, J. A. (1986). The isocon diagram: A simple solution to Gresens' equation for metasomatic alteration. *Economic Geology, 81*(8), 1976–1982. https://doi.org/10.2113/gsecongeo.81.8.1976

Gresens, R. L. (1967). Composition–volume relationships of metasomatism. *Chemical Geology, 2*, 47–65. https://doi.org/10.1016/0009-2541(67)90004-6

Han, J. S., Yao, J. M., Chen, H. Y., Deng, X. H., & Ding, J. Y. (2014). Fluid inclusion and stable isotope study of the Shagou Ag–Pb–Zn deposit, Luoning, Henan Province, China: Implications for the genesis of an orogenic lode Ag–Pb–Zn system. *Ore Geology Reviews, 62*, 199–210. https://doi.org/10.1016/j.oregeorev.2014.02.006

Harris, A. C., Golding, S. D., & White, N. C. (2005). Bajo de la Alumbrera copper–gold deposit: Stable isotope evidence for a porphyry-related hydrothermal system dominated by magmatic aqueous fluids. *Economic Geology, 100*(5), 863–886. https://doi.org/10.2113/gsecongeo.100.5.863

Hoefs, J. (2009). *Stable isotope geochemistry* (5th ed.). Springer. https://doi.org/10.1007/978-3-540-70708-0

Hofstra, M. B., Van der Ende, J., & Verhulst, F. C. (2001). Adolescents' self-reported problems as predictors of psychopathology in adulthood: 10-year follow-up study. *The British Journal of Psychiatry, 179*(3), 203–209. https://doi.org/10.1192/bjp.179.3.203

Hussain, A., Zhao, K. D., Arif, M., Palmer, M. R., Chen, W., Zhang, Q., & Girei, M. B. (2020). Geochronology, mineral chemistry and genesis of REE

mineralization in alkaline rocks from the Kohistan Island Arc, Pakistan. *Ore Geology Reviews, 126*, 103749. https://doi.org/10.1016/j.oregeorev.2020.103749

Hussain, Z., Tao, C., Li, C. F., Liao, S., Alam, M., Farhan, M., & Hussain, A. (2021). Mineralogy, fluid inclusions, and isotopic study of the Kargah Cu–Pb polymetallic vein-type deposit, Kohistan Island Arc, Northern Pakistan: Implication for ore genesis. *Minerals, 11*(11), 1266. https://doi.org/10.3390/min11111266

Jenner, G. A., Longerich, H. P., Jackson, S. E., & Fryer, B. J. (1990). ICP-MS—A powerful tool for high-precision trace-element analysis in Earth sciences: Evidence from analysis of selected USGS reference samples. *Chemical Geology, 83*(1–2), 133–148. https://doi.org/10.1016/0009-2541(90)90145-W

Kausar, A. B. (1991). *Petrology of the Kohistan Arc and hosted hydrothermal sulfides, Gilgit area, Pakistan* (Doctoral dissertation).

Kendall, B., Creaser, R. A., Gordon, G. W., & Anbar, A. D. (2009). Re–Os and Mo isotope systematics of black shales from the Middle Proterozoic Velkerri and Wollogorang formations, McArthur Basin, northern Australia. *Geochimica et Cosmochimica Acta, 73*(9), 2534–2558. https://doi.org/10.1016/j.gca.2009.01.032

Khan, M. A., Jan, M. Q., & Weaver, B. L. (1993). Evolution of the lower arc crust in Kohistan, northern Pakistan: Temporal arc magmatism through early, mature and intra-arc rift stages. *Geological Society, London, Special Publications, 74*(1), 123–138. https://doi.org/10.1144/GSL.SP.1993.074.01.09

Le, T. X., Dirks, P. H. G. M., Sanislav, I. V., Harris, C., Huizenga, J. M., Cocker, H. A., & Manestar, G. N. (2022). Quartz oxygen isotopes from the Tick Hill area in Mount Isa Inlier: Indication of a regional fluid overprint. *Australian Journal of Earth Sciences, 69*(3), 439–452. https://doi.org/10.1080/08120099.2021.1953733

Li, L., Li, S. R., Santosh, M., Zhu, J., & Suo, X. J. (2018). Early Jurassic decratonic gold metallogenesis in the eastern North China Craton: Constraints from S-Pb-C-D-O isotopic systematics and pyrite Rb-Sr geochronology of the Guilaizhuang Te-Au deposit. *Ore Geology Reviews, 92*, 558–568. https://doi.org/10.1016/j.oregeorev.2017.11.028

Li, S., Zhang, X., & Gao, L. (2019). Ore genesis at the Jinchang gold–copper deposit in Heilongjiang Province, Northeastern China: Evidence from geology, fluid inclusions, and H–O–S isotopes. *Minerals, 9*(2), 99. https://doi.org/10.3390/min9020099

Liu, Y., Chakhmouradian, A. R., Hou, Z., Song, W., & Kynický, J. (2019). Development of REE mineralization in the giant Maoniuping deposit (Sichuan, China): Insights from mineralogy, fluid inclusions, and trace-element geochemistry. *Mineralium Deposita, 54*, 701–718. https://doi.org/10.1007/s00126-018-0844-9

Mehrabi, B., Fazel, E. T., & Yardley, B. W. D. (2019). Ore geology, fluid inclusions and O–S stable isotope characteristics of the Shurab Sb-polymetallic vein deposit, eastern Iran. *Geochemistry, 79*(2), 307–322. https://doi.org/10.1016/j.chemer.2018.07.003

Mernagh, T. P., Leys, C., & Henley, R. W. (2020). Fluid inclusion systematics in porphyry copper deposits: The super-giant Grasberg deposit, Indonesia, as a case study. *Ore Geology Reviews, 123*, 103570. https://doi.org/10.1016/j.oregeorev.2020.103570

Mitchell, A. H. G., & Bell, J. D. (1973). Island-arc evolution and related mineral deposits. *The Journal of Geology, 81*(4), 381–405. https://doi.org/10.1086/627884

Ohmoto, H. (1979). Isotopes of sulfur and carbon. In H. L. Barnes (Ed.),

Geochemistry of hydrothermal ore deposits (pp. 509–567). Wiley.

Ohmoto, H. (1987). Sulfur and carbon isotopes. In H. L. Barnes (Ed.), *Geochemistry of hydrothermal ore deposits* (2nd ed., pp. 517–611). Wiley

Petterson, M. G. (2010). A review of the geology and tectonics of the Kohistan Island Arc, north Pakistan. *Geological Society, London, Special Publications, 338*(1), 287–327. https://doi.org/10.1144/SP338.13

Roedder, E. (1971). Fluid inclusion studies on the porphyry-type ore deposits at Bingham, Utah; Butte, Montana; and Climax, Colorado. *Economic Geology, 66*(1), 98–120. https://doi.org/10.2113/gsecongeo.66.1.98

Rollinson, H. R. (1993). *Using geochemical data: Evaluation, presentation, interpretation*. Longman Scientific & Technical.

Seal, R. R. (2006). Sulfur isotope geochemistry of sulfide minerals. *Reviews in Mineralogy and Geochemistry, 61*(1), 633–677. https://doi.org/10.2138/rmg.2006.61.12

Searle, M. P., & Khan, M. A. (1996). *Geological map of northern Pakistan and adjacent areas of northern Ladakh and western Tibet (1:650,000)*. Geological Survey of Pakistan.

Shah, M. T. (1994). A note on the bornite-chalcopyrite intergrowth texture in the volcanic-hosted copper mineralization in the Dir area, northern Pakistan. *Journal of Himalayan Earth Sciences, 27*(1), 125–126.

Shah, M. T., Ikramuddin, M., & Shervais, J. W. (1994). Behaviour of Tl relative to K, Rb, Sr and Ba in mineralized and unmineralized metavolcanics from the Dir area, northern Pakistan. *Mineralium Deposita, 29*, 422–426. https://doi.org/10.1007/BF00196383

Shah, M. T., & Hamidullah, S. (2000). Geology and geochemistry of the rocks of Ushiri Valley, District Dir, northern Pakistan. *Journal of Himalayan Earth Sciences, 33*(1), 53–78.

Sheppard, S. M. F., & Gustafson, L. B. (1976). Oxygen and hydrogen isotopes in the porphyry copper deposit at El Salvador, Chile. *Economic Geology, 71*(8), 1549–1559. https://doi.org/10.2113/gsecongeo.71.8.1549

Sillitoe, R. H. (2010). Porphyry copper systems. *Economic Geology, 105*(1), 3–41. https://doi.org/10.2113/gsecongeo.105.1.3

Simmons, S. F., & Brown, K. L. (2006). Gold in magmatic hydrothermal solutions and the rapid formation of a giant ore deposit. *Science, 314*(5797), 288–291. https://doi.org/10.1126/science.1132071

Sun, X., Li, R., Si, X., Xiao, K., & Deng, J. (2024). Timing and mechanism of ore precipitation in porphyry Cu systems: Insight from LA-ICP-MS analysis of fluid inclusions and in situ oxygen isotope analysis of hydrothermal quartz at the Zhunuo porphyry Cu deposit, China. *Economic Geology, 119*(3), 593–616.

Sykora, S., Cooke, D. R., Meffre, S., Stephanov, A. S., Gardner, K., Scott, R., & Harris, A. C. (2018). Evolution of pyrite trace-element compositions from porphyry-style and epithermal conditions at the Lihir gold deposit: Implications for ore genesis and mineral processing. *Economic Geology, 113*(1), 193–208. https://doi.org/10.5382/econgeo.2018.4556

Tahirkheli, T., Shah, M. T., & Khan, M. A. (1997). Lead isotopic signature of the hydrothermal copper mineralization in the Drosh–Shishi area, Chitral, Kohistan arc terrane, northern Pakistan. *Journal of Himalayan Earth Sciences, 30*(1), 209–217.

Tahirkheli, T., Shah, M. T., Khan, M. A., & Bilqees, R. (2012). Mineralogy and geochemistry of diorites and associated hydrothermal sulfide mineralization of Gawuch Formation in Drosh area, Chitral, northern Pakistan. *Journal of Himalayan Earth Sciences, 45*(1).

Trincal, V., Charpentier, D., Buatier, M. D., Grobéty, B., Lacroix, B., Labaume, P., & Sizun, J. P. (2014). Quantification of mass

transfers and mineralogical transformations in a thrust fault (Monte Perdido thrust unit, southern Pyrenees, Spain). *Marine and Petroleum Geology, 55*, 160–175. https://doi.org/10.1016/j.marpetgeo.2013.12.011

Ullah, Z., Li, H., Khan, A., Faisal, S., Dilek, Y., Förster, M. W., & Hussain, S. A. (2023). Mineralogy and PGE geochemistry of chromitites and peridotites of the Sapat Complex in the Indus suture zone, northern Pakistan: Implications for magmatic processes in the supra-subduction zone. *International Geology Review, 65*(10), 1719–1744. https://doi.org/10.1080/00206814.2022.2060715

Whitney, D. L., & Evans, B. W. (2010). Abbreviations for names of rock-forming minerals. *American Mineralogist, 95*(1), 185–187. https://doi.org/10.2138/am.2010.3371

Williams-Jones, A. E., & Migdisov, A. A. (2014). Experimental constraints on the transport and deposition of metals in ore-forming hydrothermal systems. In K. D. Kelley & H. C. Golden (Eds.), *Building exploration capability for the 21st century*.

Wilson, A. J., Cooke, D. R., Harper, B. J., & Deyell, C. L. (2007). Sulfur isotopic zonation in the Cadia district, southeastern Australia: Exploration significance and implications for the genesis of alkalic porphyry gold–copper deposits. *Mineralium Deposita, 42*, 465–487. https://doi.org/10.1007/s00126-007-0122-y

Xiao, X., Gu, L., & Ni, P. (2002). Multi-episode fluid boiling in the Shizishan copper–gold deposit at Tongling, Anhui Province: Its bearing on ore formation. *Science in China Series D: Earth Sciences, 45*, 34–44.

Yang, F., Zhai, W., Sun, X., Klemd, R., Sun, Y., Wu, Y., & Zheng, S. (2019). Fluid inclusions and stable isotopic characteristics of the Yaoling tungsten deposit in South China: Metallogenetic constraints. *Resource Geology, 69*(1), 107–122. https://doi.org/10.1111/rge.12185

Yuan, M. W., Li, L., Li, S. R., Li, C. L., Santosh, M., Alam, M., & Bao, X. B. (2019). Mineralogy, fluid inclusions and S-Pb-H-O isotopes of the Erdaokan Ag-Pb-Zn deposit, Duobaoshan metallogenic belt, NE China: Implications for ore genesis. *Ore Geology Reviews, 113*, 103074. https://doi.org/10.1016/j.oregeorev.2019.103074

Zafar, T., Rehman, H. U., Lutfi, W., Ullah, Z., Nouri, F., Sepidbar, F., & Rehman, S. U. (2023). Petrogenetic, geochemical, and geochronological constraints on magmatic evolution of the Chilas Complex gabbros, Kohistan arc, NW Himalaya. *Geological Journal, 58*(4), 1401–1427. https://doi.org/10.1002/gj.4577

Zaluski, G., Nesbitt, B., & Muehlenbachs, K. (1994). Hydrothermal alteration and stable isotope systematics of the Babine porphyry Cu deposits, British Columbia: Implications for fluid evolution of porphyry systems. *Economic Geology, 89*(7), 1518–1541. https://doi.org/10.2113/gsecongeo.89.7.1518

Zanchi, A., & Gaetani, M. (2011). The geology of the Karakoram Range, Pakistan: The new 1:100,000 geological map of Central-Western Karakoram. *Italian Journal of Geosciences, 130*(2), 161–262.

Zhai, D., Liu, J., Cook, N. J., Wang, X., Yang, Y., Zhang, A., & Jiao, Y. (2019). Mineralogical, textural, sulfur and lead isotope constraints on the origin of Ag-Pb-Zn mineralization at Bianjiadayuan, Inner Mongolia, NE China. *Mineralium Deposita, 54*, 47–66. https://doi.org/10.1007/s00126-018-0805-3

Zhai, W., Sun, X., Sun, W., Su, L., He, X., & Wu, Y. (2009). Geology, geochemistry, and genesis of Axi: A Paleozoic low-sulfidation type epithermal gold deposit in Xinjiang, China. *Ore Geology Reviews, 36*(4), 265–281.

https://doi.org/10.1016/j.oregeorev.2008.11.002

Zhang, Y. M., Gu, X. X., Liu, L., Dong, S. Y., Li, K., Li, B. H., & Lv, P. R. (2011). Fluid inclusion and H–O isotope evidence for immiscibility during mineralization of the Yinan Au–Cu–Fe deposit, Shandong, China. *Journal of Asian Earth Sciences*, *42*(1–2), 83–96. https://doi.org/10.1016/j.jseaes.2011.02.009

Zhu, X., Zhang, Q., He, Y., Zhu, C., & Huang, Y. (2006). Hydrothermal source rocks of the Meng'entaolegai Ag–Pb–Zn deposit in the granite batholith, Inner Mongolia, China: Constrained by isotopic geochemistry. *Geochemical Journal*, *40*(3), 265–275. https://doi.org/10.2343/geochemj.40.265